SAND2000-2296J

Molybdenum sources at the Alcator C-Mod divertor: measurement and modeling

D.A. Pappas, B. Lipschultz[a], B. LaBombard, and W.R. Wampler[b]

M.I.T. Plasma Science and Fusion Center, Massachusetts Institute of Technology, Cambridge, Massachusetts 02139

[a]e-mail address: Blip@PSFC.MIT.EDU

[b]Sandia National Laboratories, Dept. 1111, MS 1056, P.O. Box 5800, Albuquerque, NM. 87185-1056

Abstract

Atomic molybdenum influxes from the divertor plate in the Alcator C-Mod tokamak have been monitored using visible spectroscopy. A simple physical sputtering model has been developed, based on measurements of plasma density and temperature as well as boron influx at the divertor plate, that calculates the molybdenum source at the outer divertor. The predicted and measured Mo influxes are compared with satisfactory agreement. The sputtering due to incident deuterons, boron ions, and redeposited molybdenum is included in the calculation. The B impurity population has been found to be the dominant source of Mo sputtering. Boron flux levels were typically 0.5 % of the deuteron flux. The probability of molybdenum being "promptly" redeposited (within a gyration after having been sputtered) can be as high as 80%. The gross molybdenum erosion peaks close to the separatrix while the net erosion peaks further away along the target plate. The net erosion is low (~0.54 cm/exposure-year).

Sandia is a multiprogram laboratory operated by Sandia Corporation, a Lockheed Martin Company, for the United States Department of Energy under Contract DE-AC04-94AL85000.

1. INTRODUCTION

The choice of first wall materials, especially for the divertor, is crucial for the success of fusion devices. Apart from having a number of favorable thermodynamic and mechanical properties, the plasma facing materials should be optimized to minimize sputtering and evaporation erosion as well as tritium retention. This extends the divertor lifetime, maximizes the purity of the plasma core, and minimizes tritium inventory. Two classes of materials are used in present-day tokamaks. Low-Z divertor materials, such as beryllium and carbon, have the advantage of being fully stripped in the core, thus not radiating there. The majority of tokamaks use these materials in an attempt to minimize such radiative cooling of the core. The negative aspect of such materials comes from concerns about safety – either due to tritium retention, or from vacuum accidents where the hot graphite can lead to an uncontrollable fire. On the other hand, the use of a high-Z material, such as molybdenum or tungsten, leads to a reduction of the source generation owing to their low sputtering yields compared to low-Z materials. High-Z materials are also advantageous with respect to T retention. These characteristics have led reactor designers to choose high-Z materials for the first-wall material. However, the tokamak operational experience with such materials is minimal compared to low-Z. In order to develop more confidence in these materials we must make sure we understand the causes and magnitude of erosion at such first-wall surfaces.

Alcator C-Mod provides a unique environment for the study of the plasma interaction with a high-Z material first-wall. All of the plasma interaction surfaces in Alcator C-Mod consist of molybdenum tiles. The experiment is operated at high magnetic fields (5-8 T) and densities ($\overline{n_e} \leq 10^{21}\ m^{-3}$). Such a compact high-field device leads to high parallel power-flux densities (100-500 MW/m^2) approching that envisioned for a reactor. The vessel surfaces are boronized every 2-4 weeks during operation, depositing a monolayer of B on the Mo surfaces.

Source rate calculations have been routinely made, especially in tokamaks with low-Z plasma interaction surfaces. Two such examples are the study by Pitcher [1] for the DITE graphite limiter and by Krieger [2] for the ASDEX Upgrade carbon divertor. Calculations involving high-Z plasma interaction surfaces are fewer. Examples are the studies by Lipschultz [3] and Philipps [4] of molybdenum sputtering from the Alcator C

DISCLAIMER

limiter and Textor test limiter respectively and by Naujoks [5], which modeled tungsten as divertor target material for fusion devices.

In this work the spectroscopically-measured molybdenum sources from the outer divertor are compared to rates calculated from a standard physical sputtering model utilizing divertor Langmuir probe data and measurements of boron influx. The benchmarked model is then used to obtain information on the type of plasma discharges that contribute the most to the divertor erosion. The relative importance of the different plasma species present in causing physical sputtering is also evaluated. The campaign-integrated net erosion prediction, based on the model, is compared with net erosion measurements previously reported for a set of appropriately modified molybdenum tiles [6].

II. EXPERIMENT AND TECHNIQUE

Alcator C-Mod is normally operated with a closed single-null divertor located at the bottom of the machine [7]. Typical plasma parameters for the results presented here were I_p = 0.6-1.1 MA, $\overline{n_e} = 0.8 - 4.0 \times 10^{20}\ m^{-3}$, B_T = 5.3 T, and an elongation of 1.6. The data in this study are from Ohmic and ICRF-heated discharges (both L- and H-mode). The ICRF heating utilizes 2 two-strap antennas launching waves at 80 MHz [8]. This heats a H minority in D plasmas. The antennas are located at the outer midplane at several points around the torus. The power launched into the plasma was always ≤ 2.5 MW.

For the identification of the various molybdenum sources in Alcator C-Mod a multiple-spatial-input, absolutely calibrated, visible spectrometer was used. This system can continuously monitor emissions from up to 16 source locations with a spectral resolution of 0.15-0.25 nm and a time resolution of 56 ms. The spectroscopic determination of the molybdenum source rates was made possible by monitoring a neutral molybdenum emission line at 386.4 nm. This line is a member of a MoI triplet (λ = 379.8, 386.4, 390.2 nm), the brightest molybdenum lines observable in the operating range of the visible spectrometer. It should be noted that since the lines of interest are actually in the ultraviolet, quartz windows and fibers were used to minimize the transmission losses. The n_e and T_e profiles along the outer divertor target, necessary for

the modeling of the molybdenum sources, were measured with an array of Langmuir probes imbedded in the tiles [9].

Figure 1 shows the standard configuration for the spectroscopic views of the outer divertor together with the Langmuir probes. The neutral molybdenum particle influx, Γ, can be derived from the measured intensity I of the MoI line, using the relation [10-12]:

$$\Gamma = 4\pi I (S/XB), \quad (1)$$

where (S/XB) is the number of molybdenum ionizations per emitted photon. In the coronal approximation, this function is just the ground state ionization rate S, divided by the excitation rate X times the branching ratio B. In Eq. 1 the intensity I is in units of photons per unit time, unit area, and unit solid angle. The molybdenum source rate from the various surfaces is calculated by multiplying the molybdenum influx, Γ, by the appropriate area. In the case of the outer divertor, it is obtained by integrating, poloidally and toroidally, the molybdenum influxes over the divertor surface. This is done with the assumption of toroidal symmetry.

Appropriate *S/XB* data as a function of the plasma electron temperature and density are available for the MoI triplet from the Atomic Data and Analysis Structure (ADAS) database [13]. These data, based on a collisional-radiative model, are presented in Table 4a of Ref. [13] and can be used even in the high density limit where the simple coronal model is no longer valid. The *S/XB* values are given for a multiplet which corresponds to three lines at 379.8, 386.4, and 390.2 nm. For details of obtaining S/XB values for a single line see Appendix B of Ref. [13]. Figure 2 shows the resultant number of ionizations per emitted 386.4 nm photon as a function of the electron temperature (2a) and density (2b). The *S/XB* is very sensitive to changes of the temperature in the 1 eV to 20 eV range for all electron densities but is practically constant for temperatures above the 45 eV point. As also seen in this figure, the higher the temperature the more sensitive *S/XB* is to changes in the density. During plasma experiments, the local electron temperature and density were obtained from the Langmuir probes. Because the local plasma temperature varies inversely with the local density, the S/XB was typically in the range of 3-5.

The boron flux to the target is, as it will be shown, used in the modeling of the molybdenum source rate there. We determine this quantity from the B influx leaving the plate, under the assumption that the two are equal in this approximation of steady state.

The boron influx is determined by measuring the BII emission at 412.2 nm, included in the same spectral region as the Mo-I lines mentioned above. We again use Eq. 1 to determine the boron influx. The S/XB for this line is not in the ADAS database, but was obtained by comparison over identical shots with another B-II line at 703.2 nm, for which the S/XB data was available. The ratio of the two lines was roughly constant over a range of $n_{e,div}$ (x 3) and $T_{e,div}$ (x 5) [14]. We thus approximate the *S/XB* ratio of the two lines as a constant ($I_{703.3}$ / $I_{412.2}$ = 3.5) for all temperatures and densities.

III. MODEL

A. General description

The important elements of the erosion/redeposition model used in this study are based on the work done by Naujoks et al. [5]. Our model attributes the molybdenum sputtering to the combined action of deuterium, boron, and returning molybdenum ions impinging on the surface. The contribution from all other ions is assumed negligible. The assumption that boron is contributing to the divertor erosion is based on the observation that it is the main low-Z impurity following boronization of the Alcator C-Mod vessel. Molybdenum self-sputtering is attributed to locally produced molybdenum atoms, as will be described analytically. The model described here is based on work briefly presented earlier in Reference [15]. Here we improve on this model using experimental measurements of B influx and better descriptions of the sputtering and redeposition process.

The influx of sputtered molybdenum at the Alcator C-Mod divertor surface can be computed at each probe location by utilizing the measured ion saturation current density J_s, the inclination angle, θ (see Fig. 3), of the field lines with respect to the divertor target surface from magnetic field reconstruction [16], the local plasma characteristics (T_e, n_e) and the B influx density. The ion saturation current density, J_s, provided by the "domed" Langmuir probes [9] is the current density parallel to the magnetic field lines. To obtain the current density normal to the surface, J_s has to be multiplied by the sine of the inclination angle θ . A typical value of this angle for the Alcator C-Mod outer divertor vertical target is 0.5-1° while it is slightly larger (~2°) for the horizontal sector above the divertor nose. The (gross) molybdenum influx is calculated from

$$\Gamma = \frac{(J_S/e)}{1+\beta Z_B} \frac{Y_D + \beta Y_B}{1 - P_{pr} Y_{Mo}} \sin\theta \qquad (2)$$

where Z_B is the charge of the boron ions and Y_D, Y_B, and Y_{Mo} are the molybdenum sputtering yields due to deuterium, boron, and molybdenum ions respectively. β is the ratio of the boron to the ion flux to the target, Γ_B / Γ_D. P_{pr} is the molybdenum ion probability of 'prompt redeposition', i.e. the probability that a molybdenum ion will be redeposited within the first gyration after ionization [17,5]. (Note that the term 'prompt redeposition' is somewhat of a misnomer. This designation does not include those Mo atoms that are ionized and then immediately travel along a field line back to the surface. Such additional effects will be discussed later). The prompt redeposition effect is especially important for shallow magnetic field line inclination, as is the case in Alcator C-Mod, and for high-Z materials such as molybdenum. It should be noted that although such promptly redeposited ions may contribute in the molybdenum sputtering, this effect is ultimately beneficial in our case since the self-sputtering effect is small, and such redeposition leads to a reduction of the net erosion. The probability of prompt redeposition was calculated from [18]:

$$P_{pr} = \frac{1}{2}[\exp(-2p) + \exp(-p/5)]. \qquad (3)$$

Equation 3 is only valid for cases of shallow field line inclination [18] as is the case for the C-Mod outer divertor. The crucial parameter is the ratio p of the ionization length $\lambda_{ion} = u_{at}/(S(T_e)\, n_e)$ to the gyroradius $\rho = m_{Mo} u_{ion}/(q_{Mo}\, B)$:

$$p \equiv \lambda_{ion}/\rho \approx q_{Mo}\, B/(m_{Mo}\, S(T_e)\, n_e). \qquad (4)$$

B denotes the total local magnetic field, which is approximated by the local toroidal magnetic field, m_{Mo} and q_{Mo} the molybdenum mass and ion charge, u_{at} and u_{ion} the speed of the molybdenum neutral atom and ion respectively. $S(T_e)$ is the electron temperature dependent neutral molybdenum ionization rate which is obtained from the ADAS database [13] and [19]. To obtain Eq. 4 it was implicitly assumed that $u_{at} = u_{ion}$, which should be correct to first order, at least for singly ionized ions (q_{Mo}= e), since it is assumed that immediately after ionization the energy of the ion is not significantly different than that of the sputtered atom.

Figure 4 shows the probability of molybdenum prompt redeposition as a function

of the electron temperature for a number of electron densities. For the conditions occurring in the Alcator C-Mod divertor (typical [n_e, T_e] range for this dataset – [1×10^{19} m^{-3}, 30 eV] to [3×10^{20} m^{-3}, 5 eV]), the probability of prompt redeposition is greater than 40 % and frequently reaches values near 80 %. In this model it is assumed that all ions that are not promptly redeposited are transported away from the immediate area. The impact of this assumption will be discussed later.

B. Model Assumptions

Several other important assumptions have been made that are essential to this model. The calculation of yields is based on the revised single energy Bohdansky formula for normal incidence [20-22]. However, in tokamaks, the particle flux to the various surfaces has an energy and angular distribution. As an approximation, the bombardment will be described by a Maxwellian energy distribution at a fixed incidence angle other than normal to the surface. Firstly the appropriate yields for a normal incidence Maxwellian distribution will be calculated. At the end of this section adjustments will be made, wherever appropriate, for the angle effect.

The energy of the deuterons and boron ions at the target can be approximated by

$$E_i = 2\,T_i + Z_i \left| e\,V_S \right| + 0.5\,M_i\,c_S^2 \qquad (5)$$

The first term represents the average thermal energy per particle transported to a surface by a Maxwellian distribution of ions of temperature T_i; the second term is the energy gain of an ion with charge Z_i when falling through the sheath potential V_S; and the third term the particle flow energy at the sheath edge, or equivalently the energy gain in the presheath [23]. In the last term, M_i is the mass of the projectile and c_S is the common ion acoustic speed of all species which, for reasonably low impurity levels, is practically equal to the acoustic speed of the majority background ions (= $\sqrt{(T_i + T_e)/M_D}$, with M_D being the deuteron mass) [24]. Here, we make use of the fact that the ions enter the sheath with their acoustic speed, as required by the sheath theory [25]. We additionally assume that the boron ions are collisionally well-coupled to the deuterium ions, and thus are accelerated up to the deuterium ion acoustic speed as a result of friction with the plasma flow. This assumption should be valid for the high density conditions encountered in

Alcator C-Mod and the typical charge state of such low-Z impurities ($Z_B = 3$ as it will be described below). For simplicity, we have also used the isothermal approximation for the ion acoustic speed.

Returning to the second term of Eq. 5, it is shown by Chodura [26] that the potential drop in the sheath is independent of θ, the inclination angle of the field lines with respect to the target surface, as long as a small correction due to finite electron Larmor radius effects is neglected. What changes with θ is just the fraction of the total potential drop that occurs in the magnetic part of the sheath. The potential drop is most easily calculated in the case of electrostatic only sheath (θ = 0) [27] and is approximately equal to $eV_S = -3\,T_e$ (assuming $T_i = T_e$ and zero secondary electron emission coefficient). Equation 5 can now be rewritten as

$$\Rightarrow \quad E_i \cong (2 + 3\,Z_i + M_i/M_D)\,T_e \qquad (6)$$

The above result for the impact energy can be used in a formula given by Bohdansky to obtain the sputtering yield as a function of the temperature [20-22]. This gives a satisfactory result except in the energy threshold region where the lack of inclusion of the high energy tail of the Maxwellian distribution in the calculations results in an underestimation of the sputtering yield. For this reason, the sputtering yields used here for deuterons and boron ions are convolutions of the single energy yield curve Y(E) for normal incidence, with a Maxwellian energy distribution f(E) shifted by the energy gained from the sheath potential, $3\,Z_i\,T_e$, and in the presheath $(M_i/M_D)\,T_e$. $T_i = T_e$ was again assumed and $E_{Sheath} = 3Z_iT_e + (M_i/M_D)T_e$ was used.

Such a description is valid only for deuterium and boron projectiles reaching the target. For the calculation of the molybdenum self-sputtering yield we need to have an estimate of the energy of the molybdenum ions returning to the divertor surface. Since only promptly redeposited molybdenum ions are considered, they do not have the time to reach thermal equilibrium. Hence the energy of the molybdenum ions will be the sum of the original energy of the sputtered atoms plus the energy gained in the sheath, which depends on where the molybdenum atoms are ionized with respect to the beginning of the sheath. Since the threshold for molybdenum self-sputtering is 64 eV [21], the original energy of the sputtered molybdenum atoms, which is a few eV [28], can be neglected

without introducing a significant error. In the current model, molybdenum is assumed, for simplicity, to be ionized just outside the sheath, gaining the full energy of 3 Z_{Mo} T_e on returning to the surface. Figure 5 shows the neutral molybdenum ionization mean free path as a function of the electron temperature for a number of electron densities. The magnetic sheath size, which is of the order of the background plasma ion gyroradius [26] and much larger than the electrostatic part of the sheath (~ 10 Debye lengths [26]), is also plotted as a function of temperature. A survey of typical C-Mod divertor conditions shows that molybdenum is typically ionized at a distance from the plate 1-2 x the magnetic sheath thickness. Hence, for the calculation of the self-sputtering yield, the single energy Bohdansky formula for normal incidence is used with the assumption that all molybdenum ions have energy 3 Z_{Mo} T_e.

To complete the calculation of the energy gained inside the sheath by boron and molybdenum ions we need to have an idea of what their average charge state is. Boron ions are assumed to be helium-like (i.e. $Z_B = +3$). This choice is supported from previous calculations and experiments. Post et al. have calculated the average charge state as a function of the electron temperature for a number of elements [29]. The average boron charge is 3 for temperatures in the range 5 to 30 eV which is typical for C-Mod conditions. In addition, Matthews et al. have found, using plasma ion mass spectrometry on the DITE tokamak, that the fluxes of impurities such as carbon and oxygen are very similar in all charge states up to their helium-like states [30]. An even more relevant measurement is that of Nachtrieb [31] who recently measured significant levels of helium-like boron in Alcator C-Mod. Specifically, in a rather cold region (T_e < 10 eV) of the scrape-off-layer, he determined that the helium-like boron flux is ~ 2 % of the deuteron flux.

For the promptly redeposited Mo ions an average charge $Z_{Mo} = +1.5$ is used. This is based on the fact that at high electron densities, such as is the case for Alcator C-Mod, particles can be ionized multiple times before completing their first orbit [5]. Although these additional ionizations will reduce the probability of prompt redeposition, some of the ions will make it back to the target. This assumption is further supported by a calculation, by Brooks and Ruzic, for tungsten in a D-T background plasma with parameters similar to C-Mod (magnetic field 5 T, $n_e \sim 10^{20}\ m^{-3}$, $T_e \sim 30$ eV, inclination

angle $\theta = 3^\circ$) in which an average charge of 2.1 is obtained for the redeposited ions [32]. With the above choices for the charge of boron and molybdenum ions, the typical energies with which the various projectiles arrive at the plate are (from Eq. 6): 6 T_e for deuterons, 16.4 T_e for boron ions, and 4.5 T_e for molybdenum ions.

Up to this point only the yields for normal incidence have been calculated. However no adjustment needs to be made to the molybdenum sputtering yields due to deuterium and boron ions despite the fact that their average angle of incidence is actually $\alpha = 65^\circ$ [33]. The reason is that for light ions incident on heavy targets, the sputtering yield for the energies of interest at $\alpha = 65^\circ$ is close to the yield at normal incidence [34].

Sputtering models have shown that a different set of parameters characterize heavy ion sputtering of heavy targets. Brooks and Ruzic have found, in the same calculation that provided the average charge of redeposited tungsten, that sputtered tungsten ions tend to impact at near normal angles of incidence ($\alpha \approx 18^\circ$) [32]. Since no data were available regarding the dependence on the angle of incidence of the Mo self-sputtering yield, the corresponding (for $\alpha \approx 18^\circ$) yield enhancement for tungsten self-sputtering as a function of the ion energy [28] was applied to the Mo self-sputtering. Figure 6 shows the enhancement applied to the molybdenum self-sputtering yield for normal incidence as a function of the projectile energy.

The necessary parameters Q (yield factor), E_{th} (threshold energy), and E_{TF} (Thomas-Fermi energy), for the calculation of the yields have been tabulated for the elements of interest with the exception of boron [21]. In that case we use analytic expressions for Q and E_{th} [22] and E_{TF} [21]. A summary of all the parameters used in the calculation of the molybdenum yields is given in Table 1. The sputtering yields of interest, as calculated based on the assumptions described in this section, are plotted as a function of the temperature in Fig. 7. Fig. 7a shows the yields for bombardment with deuterium and triply ionized boron ions and Fig. 7b the self-sputtering yield for molybdenum ions redeposited at $\alpha = 18^\circ$. (The self-sputtering yield for $\alpha = 0^\circ$ is also shown for comparison). The sputtering yield due to deuterium ions is much lower than that due to the triply ionized boron ions. Hence, even at low boron concentrations, molybdenum sputtering by boron would be significant at all temperatures. It would actually dominate sputtering for temperatures $T_e \leq 20$ eV. Self-sputtering is significant

for $T_e \geq 15$ eV under the assumptions made here regarding charge state. However, it does not become dominant for any of the conditions that are typically encountered in the Alcator C-Mod divertor.

Finally, it has already been mentioned that the boron flux to the target is inferred from the spectroscopically measured brightness of the 412.2 nm BII line. The deuteron flux is obtained from the probe data and approximated with $\Gamma_D = (J_S / e) \sin\theta$.

IV. COMPARISON OF THE MODEL WITH SPECTROSCOPY

There are seven probes located on the vertical face of the outer divertor. Six chordal spectroscopic views of this same surface were used during the experiments described here (see Fig. 1). The total Mo source rate, Φ, is obtained by integrating the Mo influxes over the divertor surface for both the model and the experiment. A comparison of the two results for an entire shot is shown in Fig. 8. Good agreement can be seen during the ohmic part of the shot. During the RF phase, the sputtering model predicts values ~ 2 times higher for the molybdenum source. This higher model prediction is not repeatable. There are also shots with better quantitative agreement during the ohmic phase.. However, for the majority of shots, the temporal behavior of both results is similar, signifying that the model incorporates most of the appropriate physics.

Similar results are also observed in individual chord and probe comparisons as seen by looking at Fig. 9. Figure 9 shows the molybdenum influxes measured with the spectrometer views # 8, # 10, # 12, # 14, # 16, and # 18 of Fig. 1 and the corresponding influxes calculated from probes # 2 through # 7 for the same discharges shown in Fig. 8. (Recall from Fig. 1 that there is essentially a one to one correspondence between these six views and probes, with view # 8 corresponding to probe # 2, view # 10 to probe # 3, etc). The agreement is fairly good for most of the probe-view pairs. There is, however, a significant discrepancy between the two results at the lower part of the outer divertor during the RF phase. The high molybdenum influx calculated from the # 2 probe data dominates the total divertor molybdenum source during this period and is the cause of the model overestimation of the source rate that was initially observed in Fig. 8. This increased calculated molybdenum influx at probe # 2 comes as a result of the combined high boron flux fraction and deuteron flux to the target during the RF phase in the

vicinity of the specific probe and the increase in local temperature.

The results of such cases as Fig. 8 can also be integrated over an entire discharge. Figure 10 shows a comparison between model and spectroscopy for a number of discharges from a particular run. These discharges have widely varying conditions, including different plasma currents and volume averaged electron densities. They have been selected because among them are included those with the highest measured molybdenum source rates during the 1995-1996 run period. (This run period data was used for comparison with the model because, later in this paper, we will compare model predictions of integrated erosion to direct measurements of surface erosion, only available for that run period) The molybdenum source rate averages during the ohmic phase of the shots are plotted in the top panel (a) while the averages during the RF phase are plotted in the lower panel (b). The ohmic and RF averages are plotted as a function of the sequential shot number, starting from the beginning of this run day. Before reaching any conclusions from this graph, the following point should be made: the vessel was boronized just prior to this run day and the effect of the boronization is revealed in the figure. Specifically, it is shown that the spectroscopically-measured sources were lower than the calculated ones during the beginning of the run day. This is because immediately following boronization of the chamber, a thin (~ 100 nm) boron layer covers all molybdenum surfaces. This causes the molybdenum emissions, from all locations observed, to be practically zero. The measured divertor molybdenum influx recovers to close to original levels as the day progresses and the boron layer is eroded. However, no corrections are made in the model with regards to boronization. The model calculates the sputtering assuming a 100 % molybdenum surface, based on the measured temperatures and densities, and hence it would predict higher molybdenum sputtering than measured, as long as the boronization is still effective.

Looking at the rest of the shots in Fig. 10, it is seen that there is a satisfactory quantitative agreement between the two results in the ohmic phase but poorer matching during the RF phase. As discussed earlier, in reference to Fig. 8, this observation can not be generalized since there are data from other discharges where the agreement is better during the RF phase. In general, the match in trends and magnitude exemplified in Fig. 10 are typical of the close to 250 shots analyzed.

It is of interest to know what the typical levels for the boron flux fraction that are used in the model are. In Fig. 11, the distribution of the divertor averaged boron flux fraction ($\Sigma\Gamma_B / \Sigma\Gamma_D$) for the ohmic and RF phase of 67 C-Mod discharges is plotted. As seen there, both curves exhibit a maximum in the region of a boron flux fraction of 0.5 %.

V. DISCUSSION

A. Evaluation of the model

The physical sputtering model described in the previous sections has provided satisfactory agreement with the spectroscopic results, signifying a fairly good understanding of the mechanism responsible for the generation of molybdenum at the outer divertor plates. However, there are some points that need further investigation that will be discussed in this section.

In the discussion regarding the yields for the various species used in this model (see Fig. 7), it was noted that boron sputtering of molybdenum was expected to play an important role and actually dominate for temperatures below 20 eV. Figure 12 shows the contribution of the various projectiles to the molybdenum source rate for two shots. Note that the shot in Fig. 12a is the one analyzed in the previous section (Figs. 8 and 9). In this discharge, the boron clearly dominates the molybdenum sputtering. This can be mainly attributed to the relatively low temperatures in the divertor during this shot. In the discharge shown in the bottom panel (Fig. 12b), the contribution from the other species, especially deuterium, is bigger, becoming at certain times comparable to that of boron. At all times, the contribution of the promptly redeposited molybdenum ions is the smallest. These results are representative of the findings for all shots. Boron contributes the most to the sputtering while self-sputtering does not typically exceed 25 % of the total calculated source rate.

An important assumption in our model is the inclusion of only promptly redeposited molybdenum ions in the self-sputtering calculation. Although the probability of prompt redeposition frequently reaches values close to 80% for the conditions occurring in C-Mod plasmas, it was important to investigate the effect of the rest of the

molybdenum ions. Two cases were considered. First, the extreme case in which all those ions ($1\text{-}P_{pr}$) are assumed to be collisionally well-coupled to the background plasma and return to the surface where they originated from. For the calculation of the molybdenum source rate, Eq. 2 was modified as follows:

$$\Gamma_{gross} = \frac{(J_S/e)}{1+\beta Z_B} \frac{Y_D + \beta Y_B}{1 - P_{pr} Y_{Mo} - (1-P_{pr}) Y'_{Mo}} \sin\theta \,. \qquad (7)$$

In the above equation, Y'_{Mo} is the sputtering yield due to the non-promptly redeposited molybdenum ions. The energy of these ions was calculated using Eq. 6. However, for molybdenum ions collisionally well-coupled to the background plasma, their flow speed will approach that of the background D ions. This would result in a flow energy that is enormous, approximately 48 T_e. This approach leads to nonphysical results, with the calculated molybdenum source rate substantially higher than that found with spectroscopy. It would also mean that the molybdenum ions, after being ionized close to the plate, must then be transported away from the plate (against the flow) allowing time to be collisionally coupled to the flow (towards the plate).

A more realistic case was then investigated: Eq. 7 was again used for the calculation of the molybdenum source rate but now the non-promptly redeposited molybdenum ions are not considered to be flowing towards the target at the deuteron sound speed. Since the sheath is collisionless it is probable that molybdenum ions, which are ionized just outside the sheath, do not have time to equilibrate with the deuterons moving at the sound speed. In neglecting the directed flow energy, we still conservatively assumed that the charge of these ions was 3 and hence they gain an energy 9 T_e as a result of the acceleration inside the sheath. The result was that the additional sputtering contributed by those Mo ions that are not promptly redeposited ($1\text{-}P_{pr}$) did not typically exceed 15 % of the total from other sputtering sources (including self-sputtering from promptly redeposited Mo). Hence, neglecting them was a reasonable and practical assumption given the goals of this study.

The variable discrepancy between the measured and modeled molybdenum source rate results is a source of concern. One potential source of error is the boron flux to the target. It is difficult to estimate the uncertainty associated with this parameter. However, such a systematic error would likely lead to a general under- or over-estimate of the

sputtering rate, not variable as observed.

During the RF phase, the molybdenum source rate is often underestimated by the model. There are many mechanisms that can be employed to explain it. The probe and MoI spectroscopic measurements are made at two separate toroidal locations. It is possible that the level of toroidal asymmetry (unknown) changes upon transition to the RF phase of a discharge. However, we have no evidence that would support such a possibility.

Another possible explanation of the discrepancy between model and molybdenum source measurements during RF heating is that the energy of sputtering ions is somehow enhanced in the presence of RF heating. This could occur due to either the emergence of a non-thermal electron population or an increase in T_i/T_e. The former increases the sheath potential even in the presence of very small (~1%) non-thermal populations [35]. The latter directly affects the energy of the ion and is, perhaps, more likely to be the cause of the discrepancy. While this requires further investigation, it is important to note that energetic ion particle tails of up to 4 keV have been observed in the plasma edge of Alcator C-Mod during RF heating [36].

B. Discharges which Contribute the most to Divertor Erosion

It is of great importance to identify the type of discharges that cause most of the observed erosion in the divertor surfaces. In particular, it is crucial to understand the effect of the various plasma parameters on the divertor erosion. This may help provide some insight into minimizing erosion, or equivalently, maximizing the lifetime of the divertor surfaces. Spectroscopic information on the molybdenum sources is not always available due to the use of the spectrometer in a variety of experiments, which necessitates changing the spectral coverage to a range not including the molybdenum lines of interest. This prohibits us from having complete information for all type of discharges. On the other hand, based on the satisfactory agreement between model and spectroscopy, we can use the model to obtain divertor erosion information for most of the shots during an experimental campaign. The erosion can always be calculated as long as divertor probe data, and information on local magnetic field orientation, are available, which is typically the case. For this reason, the outer divertor molybdenum gross erosion

was calculated for almost all shots of the 1995-1996 run campaign. Specifically, the molybdenum source rate was calculated (using Eq. 2) for all shots with available probe data as a function of time and it was then integrated over the duration of each shot to give the total gross erosion (in molybdenum atoms). It should be noted that this calculation, as well as the one described in the next section, had been performed using a constant boron flux fraction of 0.5 % based on the results shown in Fig. 11. The reason for this approach is that the calculation of the boron flux to the target is based on the spectroscopic measurement of the boron emission at 412.2 nm which, like the molybdenum source rate measurement, is not available for all shots. In addition, an extra arbitrary factor of 2 was used to artificially correct the systematic underestimation of the calculated molybdenum source rate during the RF phase (for RF powers greater than 1.1 MW) which is in most cases observed *when a constant boron flux fraction is used* [15]. Of course all results are subject to the problems mentioned in the previous sections regarding the performance of the model. However, since we are dealing with a large number of shots, and the effect of boronization on the outer divertor is not long lasting, the model should still be able to reveal all the important parameters that influence the erosion levels.

A total of 944 shots were analyzed. The shots are separated into groups based on their plasma current. A shot is included in a specific group as long as its current falls within $\pm$ 50 kA of the nominal plasma current for the group. For example all shots with plasma currents ranging from 550 kA to 650 are considered as "600 kA" discharges. The majority of shots from the 1995-1996 campaign are included in one of the following four plasma current groups: 600 kA, 800 kA, 1000 kA, and 1100 kA.

Tables 2 - 4 summarize the most important findings with regard to the effect of the plasma current and the RF power on the divertor gross erosion. Table 2 summarizes both the ohmic and RF phases of all of the shots from this run period. It provides the number of shots for each plasma current level, their fraction with respect to the total, the total gross erosion for the shots of that current level, and the fraction with respect to the total calculated erosion for all 944 shots. Table 3 provides the average erosion per shot for just the ohmic phase of the shots. Although the electron density varied widely, the average plasma density for each current group was approximately constant. It is evident that the erosion increases significantly with increasing plasma current. For a set of ohmic

discharges of constant density, higher plasma current would lead to higher power flowing into the scrape-off-layer (SOL) and thus higher divertor temperatures. Application of a simple two-point model [37] to the increased SOL power flow leads to increased sputtering yields consistent with the scaling seen in table 3.

Table 4 describes the effect of the RF power on the outer divertor erosion by giving the fraction of the time that the RF was on for each plasma current and the corresponding erosion fraction for the specific current. Clearly, for all currents, most of the outer divertor gross erosion occurs during the RF phase of plasma discharges.

The effect of the electron density on the gross erosion was also investigated. Although there is a general trend at the various plasma currents for the erosion to decrease with increasing density the spread in the data was too big to obtain any other useful conclusions.

Another way of looking at the data is to plot the total (for all 944 shots) gross erosion at the 10 outer divertor probes. This is done in Fig. 13a where the total gross erosion as well as the erosion occurring during the RF heating phase are plotted versus the distance of the 10 probes from the midplane (probe 1 is the furthest away from the midplane, see Fig. 1). In Fig. 13b the erosion fraction during RF portions of the discharge is plotted based on the ratio of the curves from the top panel. The erosion (in units of material thickness) for each shot was obtained by integrating the molybdenum influx over the duration of the shot and dividing by the molybdenum atom density. The gross erosion peaks in the vicinity of the outer strike point. The erosion occurring during the RF phase of the discharges (25-30% of the overall discharge period – see Table 4) dominate the erosion at the lower part of the plate. The peaking of the erosion during the RF phase in the area of the separatrix can be understood as follows: addition of RF power raises the power flow into the SOL, raising the divertor T_e. In most shots with sufficient RF power, the plasma would go into an H-mode (with the main exception being shots at the beginning of a run campaign when the vessel is not well-conditioned). In H-mode, the scrape-off-layer width decreases considerably. The narrower heat flux profile and higher divertor T_e imply that most of the target erosion would occur in the vicinity of the separatrix.

C. Calculated vs. Measured Divertor Erosion

During the 1995-1996 experimental campaign the total molybdenum net erosion at various locations inside the C-Mod vessel was measured with the use of appropriately modified molybdenum tiles [6]. In these tiles, a layer of chromium was planted underneath the surface and used as a depth marker. The depth of the chromium layer beneath the surface was measured by Rutherford backscattering before and after the tiles were exposed to plasma discharges. A total of 21 such tiles were used in areas such as the inner wall, and the inner and outer lower divertor. The tiles were installed before the beginning of the run campaign and were exposed to 1090 tokamak pulses during the period from November 1995 to March 1996. Examination of the tiles after the exposure showed significant net molybdenum erosion only at the outer divertor and much less, if any, everywhere else (e.g. inner divertor, inner wall).

The outer divertor net erosion measurements have been compared with a campaign-integrated net erosion prediction, based on the model assumptions already discussed and probe measurements. The net erosion is calculated by multiplying the gross erosion, Eq. 2, by the fraction of the atoms that did not promptly redeposit, $(1 - P_{pr})$. Data from 990 shots were used in this calculation. The lack of data in the remaining 100 shots is not a cause of concern. These are mainly short-period shots, many of them shortly after a vacuum break, that were not diverted at all. Figure 14 shows the probe-deduced campaign-integrated gross and net erosion together with the net erosion as determined from the marker tiles as a function of the distance of each of the ten probes below the midplane (Fig. 14a). It also shows the contribution of the various projectiles used in the model to the total calculated gross erosion (Fig. 14b). As shown in the figure, there is generally good qualitative agreement between the measured and calculated net erosions while quantitatively they differ, depending on the location, at most by a factor of about 3. From Fig. 14b it is clear that the gross erosion is dominated by boron. It should be noted that the D ion contribution includes the enhancement of the calculated gross erosion by a factor of 2 during RF heating, that was mentioned in the previous section.

The difference in the location of the peaks between the gross and the net erosion profiles is striking. The gross erosion, as already seen, peaks in the vicinity of the separatrix while the net erosion away from it and actually in the area of the divertor nose.

This result was expected since the molybdenum prompt redeposition is very strong close to the separatrix and much lower further away, where the mean free path for ionization is longer due to the lower values of density and temperature.

Looking at the net measured (or calculated) erosion results, useful information can be extracted for the usage of high-Z materials in the divertor region. With the peak molybdenum measured erosion being about 170 nm for a total exposure of about 1000 s, the average erosion is only 0.17 nm/s or 0.54 cm/exposure-year. This is not only very small in terms of absolute numbers but is also much lower than erosion rates (> 10 cm/exposure-year) measured for graphite tiles at the outer divertor region in the DIII-D tokamak [38]. This is consistent with the lower molybdenum sputtering yields. In addition, one could make a very simple, order of magnitude estimate of the net erosion expected in an ITER-like machine having high-Z divertor target plates. Assuming that the density in the vicinity of the divertor target in this future machine is 4x higher than in Alcator C-Mod and the temperature similar, then the peak net erosion for a single shot lasting 1000 s will be ~ 700 nm. Then for a campaign lasting a 1000 shots, the peak net erosion will be ~ 700 μm. These numbers are very small and hence encouraging. If they will be true in a future machine, then they imply that physical sputtering will not be a major source of concern for the integrity of the divertor.

VI. CONCLUSIONS

Measured molybdenum sources at the outer divertor in Alcator C-Mod are in good agreement with the ones calculated from a simple physical sputtering model. The effect of deuterons, boron ions, and promptly redeposited molybdenum ions incident on the target is included in the calculation. The deuteron flux to the target was calculated from Langmuir probe data while the boron flux was estimated from spectroscopic measurements of boron emissions. Boron flux levels were typically 0.5 % of the deuteron flux. The model showed that the molybdenum sputtering is dominated by the boron ions. It was also found that the molybdenum ion probability of prompt redeposition is high, reaching, under typical C-Mod conditions, values as high as 80 %, which leads to a significant reduction in the net target erosion. Specifically, it has been found that although the molybdenum gross erosion peaks close to the separatrix, the net erosion,

which is rather small in absolute numbers, peaks further away in the target plate. The latter is also consistent with erosion measurements performed in C-Mod with appropriately modified molybdenum tiles. The molybdenum that is not promptly redeposited is ionized close to the sheath edge, making it likely that is quickly redeposited as well, which would lead to a further reduction of the net erosion.

The divertor source model has also been used to investigate the effect of various plasma parameters on the molybdenum source rate levels. Analysis of a large number of discharges showed that the molybdenum source rate increases significantly with both the plasma current and with the application of RF power.

ACKNOWLEDGEMENTS

The authors would like to thank the entire Alcator group for their efforts in producing the discharges used for this work. The authors gratefully acknowledge helpful discussions with P.C. Stangeby, G.M. McCracken and C.S. Pitcher. This work supported by the U.S. Department of Energy under grant DE-FC02-99ER54512.

Table Captions

Table 1: Parameters used in the model for the calculation of the molybdenum sputtering yield. E_{th}, E_{TF}, and Q for D and Mo are from Ref. [21].

Table 2: General description for each plasma current range: the fraction of discharges at each plasma current value, the integrated erosion over those shots, and the fraction of the total erosion.

Table 3: Dependence of the average calculated outer divertor gross erosion on the plasma current for the ohmic phase of plasma discharges.

Table 4: Effect of RF power on the calculated outer divertor gross erosion.

Figure Captions

Fig. 1: Poloidal cross section of the divertor region. The divertor spectroscopic views use local electron temperature and density obtained with the divertor Langmuir probes. A typical plasma separatrix is also drawn.

Fig. 2: Molybdenum ionizations per 386.4 nm emitted photon (*S/XB*) as a function of the electron temperature (a) and density (b).

Fig. 3: Schematic view of an ion's trajectory in the proximity of the divertor surface. The ions spiral around the magnetic field up to the beginning of the (magnetic) sheath. Inside the sheath, the electric field tends to pull the plasma flow closer to the direction of the normal to the target [33].

Fig. 4: Probability (based on Eq. 3) of molybdenum prompt redeposition as a function of the electron temperature for a number of electron densities.

Fig. 5: Neutral molybdenum ionization mean free path as a function of the electron temperature for a number of electron densities. The magnetic sheath size is also plotted as a function of temperature.

Fig. 6: Molybdenum self-sputtering yield enhancement, with respect to the yield for the target at $\alpha = 0^{\circ}$. The data used, are a fit to calculated data for tungsten [28].

Fig. 7: Molybdenum sputtering yields as a function of the temperature for bombardment with deuterium and triply ionized boron projectiles having a Maxwellian energy distribution (a). The yields are calculated for normal incidence since $Y(\alpha = 65^{\circ}) \sim Y(\alpha = 0^{\circ})$. Also shown (b) is the molybdenum self-sputtering yields used for the promptly redeposited projectiles of energy $4.5\ T_e$, incident at $\alpha = 18^{\circ}$. The self-sputtering yield for normal incidence ($\alpha = 0^{\circ}$) is given for comparison.

Fig. 8: Comparison of the calculated outer divertor source rate from spectroscopic data and the sputtering model. The RF power, indicated by shaded region, is increased from 1.2 to 1.6 MW at 0.95 s.

Fig. 9: Comparison of the spectroscopically measured molybdenum influx, for the six outer divertor chords used, to that calculated from the sputtering model for the corresponding probes.

Fig. 10: Molybdenum source rates from spectroscopy and model for a number of shots from one run: a) averages during the ohmic phase of each shot; b) averages during the RF phase.

Fig. 11: Distribution of divertor averaged boron flux fraction ($\Sigma\Gamma_B / \Sigma\Gamma_D$ over divertor / divertor) for the ohmic and RF phase of 67 C-Mod discharges.

Fig. 12: Contribution of the various projectiles used in the model to the calculated molybdenum source rate. The data from two representative shots are given in panels a and b.

Fig. 13: a) Total gross erosion and gross erosion during RF heating as a function of the position on the outer divertor target. b) the RF erosion fraction at the same places.

Fig. 14: a) Outer divertor campaign-integrated model (gross and net) erosion and measured (net) erosion, from Reference [6], as a function of the distance from the midplane for each of the ten probes. b) Contribution of the various projectiles used in the model to the total calculated gross erosion.

Table 1

Projectile	D	B	Mo
E_{th} (eV)	90	26.8	64
E_{TF} (eV)	4767	27825	533048
Q (atoms/ion)	0.023	1.28	18
Z	1	3	1.5
α	65^0	65^0	18^0

Table 2

Ip (kA)	Shots	Shot fraction (%)	Total erosion below nose (Mo. Atom)	Erosion fraction (%)
600	83	8.8	3.12×10^{20}	4.8
800	404	42.7	1.97×10^{21}	30.6
1000	199	21.1	2.79×10^{21}	42.1
1100	78	8.3	1.31×10^{21}	20.2
All I_p	944		6.46×10^{21}	

Table 3

Ip (kA)	600	800	1000	1100
Erosion per shot (atoms)	1.35×10^{18}	2.7×10^{18}	5.74×10^{18}	7.74×10^{18}

Table 4

Ip (kA)	Time RF on (fraction of total, %)	Erosion during RF (fraction of total, %)
600	27.1	69.1
800	18.7	40.3
1000	33.1	64.6
1100	29.4	56.5
All I_p	22.2	56.3

REFERENCES

[1]C. S. Pitcher, G. M. McCracken, D. H. J. Goodall, A. A. Haasz, G. F. Matthews, and P. C. Stangeby, Nucl. Fusion **26**, 1641 (1986).

[2]K. Krieger, J. Roth, A. Annen, W. Jacob, C. S. Pitcher, W. Schneider, A. Thoma, and M. Weinlich, J. Nucl. Mater. **241-243**, 684 (1997).

[3]B. Lipschultz, B. LaBombard, E.S. Marmar, M.M. Pickrell, and J.E. Rice, J. Nucl. Mater. **128-129**, 555 (1984).

[4]V. Philipps, T. Tanabe, Y. Ueda *et al.*, Nucl. Fusion **34**, 1417 (1994).

[5]D. Naujoks, K. Asmussen, M. Bessenrodt-Weberpals *et al.*, Nucl. Fusion **36**, 671 (1996).

[6]W. R. Wampler, B. LaBombard, B. Lipschultz, G. M. McCracken, D. A. Pappas, and C. S. Pitcher, J. Nucl. Mater. **266-269**, 217 (1999).

[7]I. H. Hutchinson, R. Boivin, F. Bombarda *et al.*, Phys. Plasmas **1**, 1511 (1994).

[8]S. N. Golovato, M. Porkolab, Y. Takase *et al.*, in Radio Fequency Power in Plasmas (Proc. of the 11th Topical Conf., Palm Springs, Ca. U.S.A., 1996), Radio Fequency Power in Plasmas series, Vol. 355, AIP New York (1996) 23-30.

[9]B. LaBombard, J. Goetz, C. Kurz *et al.*, Phys. Plasmas **2**, 2242 (1995).

[10]K. Behringer, H. P. Summers, B. Denne, M. Forrest, and M. Stamp, Plasma Phys. Control. Fusion **31**, 2059 (1989).

[11]G. Fussmann, J. V. Hofmann, G. Janeschitz, and H. R. Yang, Nucl. Fusion **30**, 2319 (1990).

[12]A. R. Field, C. Garcia-Rosales, G. Lieder, C. S. Pitcher, and R. Radtke, Nucl. Fusion **36**, 119 (1996).

[13]N. R. Badnell, T. W. Gorczyca, M. S. Pindzola, and H. P. Summers, J. Phys. B: Atom. Mol. & Opt. Phys. **29**, 3683 (1996).

[14]D. A. Pappas, "Study of molybdenum sources and screening in the Alcator C-Mod tokamak," Ph.D., Report PSFC/RR-00-6, Massachusetts Institute of Technology, 2000.

[15]D. A. Pappas, B. Lipschultz, B. LaBombard, M. J. May, and C. S. Pitcher, J. Nucl. Mater. **266-269**, 635 (1999).

[16]L. L. Lao, H. St. John, R. D. Stambaugh, A.G. Kellman, W. Pfeiffer, and Nucl. Fusion 25 (1985) 1611, Nucl. Fusion **25**, 1611 (1985).

[17]G. Fussmann, W. Engelhardt, D. Naujoks *et al.*, in IAEA conference (Proc. of the 15th Conf. on Plasma Phys. & Contr. Nucl. Fusion Res., Seville, Spain, 1994), IAEA conference series, Vol. 2, IAEA (1994) 143.

[18]D. Naujoks, Nucl. Fusion **37**, 1193 (1997).

[19]M. J. Higgins, M. A. Lennon, J. G. Hughes, K. L. Bell, H. B. Gilbody, A. E. Kingston, and Culham Abingdon U. K. Smith Fj. Ukaea, 'Atomic and molecular data for fusion. 3. Recommended cross sections and rates for electron impact ionization of atoms and ions: copper to uranium', Culham report# CLM-R294, 1989.

[20]J. Bohdansky, Nucl. Instr. & Meth. in Phys. Res. B - Beam Interactions with Atoms **2**, 587 (1984).

[21]W. Eckstein, J. Bohdansky, and J. Roth, Atomic & Plasma Material Interaction Data for Fusion, Supplement to the journal Nuclear Fusion **1**, 51 (1991).

[22]C. Garcia-Rosales, W. Eckstein, and J. Roth, J. Nucl. Mater. **218**, 8 (1995).

[23]P. C. Stangeby, J. Phys. D - Appl. Phys. **20**, 1472 (1987).

[24]P. C. Stangeby, Phys. Fluids **30**, 3262 (1987).

[25]P. C. Stangeby and G. M. McCracken, Nucl. Fusion **30**, 1225 (1990).

[26]R. Chodura, "Plasma flow in the sheath and presheath of a scrapeoff layer," in *Physics of Plasma-Wall Interactions in Controlled Fusion.*, edited by D. E. Post and R. Behrisch (Plenum Press, New York, 1986), pp. 99-134.

[27]P. C. Stangeby, "The plasma sheath," in *Physics of Plasma-Wall Interactions in Controlled Fusion.*, edited by D. E. Post and R. Behrisch (Plenum Press, New York, 1986), pp. 41-97.

[28]W. Eckstein and V. Philipps, "Physical sputtering and radiation-enhanced sublimation," in *Physical processes of the interaction of fusion plasmas with solids*, edited by W. O. Hofer and J. Roth (Academic Press, 1996), pp. 93-134.

[29]D. E. Post, R. V. Jensen, C. B. Tarter, W. H. Grasberger, and W. A. Lokke, Atomic Data & Nuclear Data Tables **20**, 397 (1977).

[30]G. F. Matthews, R. A. Pitts, G. M. McCracken, and P. C. Stangeby, Nucl. Fusion **31**, 1495 (1991).

[31]R. T. Nachtrieb, B. LaBombard, and E. Thomas, 'Omegatron ion mass spectrometer for the Alcator C-Mod tokamak.', M.I.T. report# PSFC/JA-00-3, 2000, to be published in Rev. Sci. Instrum.

[32]J. N. Brooks and D. N. Ruzic, J. Nucl. Mater. **176-177**, 278 (1990).

[33]R. Chodura, J. Nucl. Mater. **111-112**, 420 (1982).

[34]J. P. Biersack and W. Eckstein, Applied Physics A: Solids and Surfaces **34**, 73 (1984).

[35]P. C. Stangeby, Plasma Phys. Control. Fusion **37**, 1031 (1995).

[36]J. C. Rost, "Fast ion tails during radio frequency heating on the Alcator C-Mod tokamak," Ph.D., Report PSFC/RR-98-3, Massachusetts Institute of Technology, 1998.

[37]C. S. Pitcher and P. C. Stangeby, Plasma Phys. Control. Fusion **39**, 779 (1997).

[38]D. G. Whyte, J. N. Brooks, C. P. C. Wong, W. P. West, R. Bastasz, W. R. Wampler, and J. Rubenstein, J. Nucl. Mater. **241-243**, 660 (1997).

Figure 1

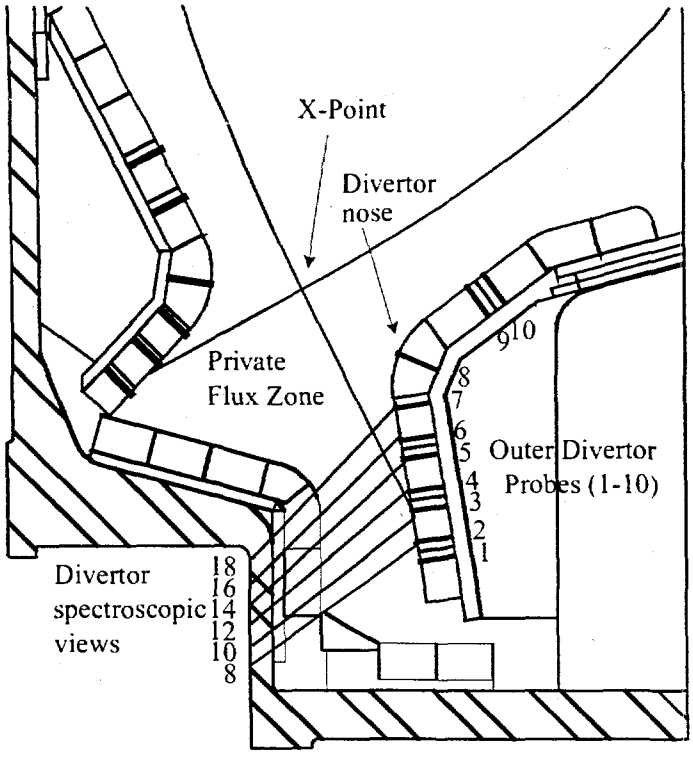

Figure 2

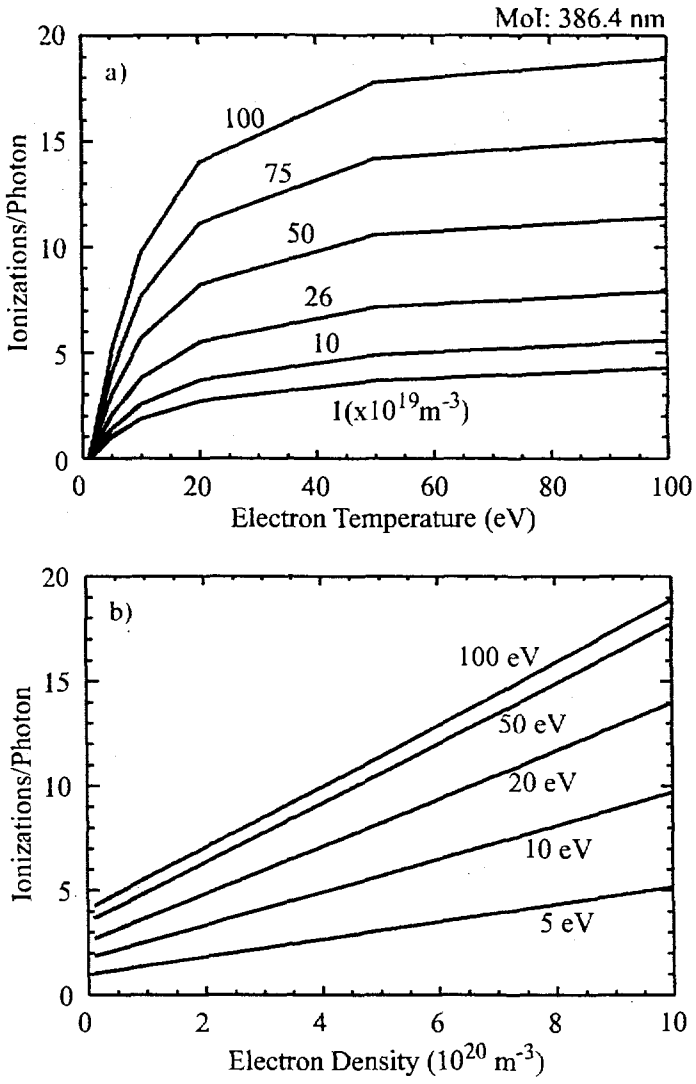

Figure 3

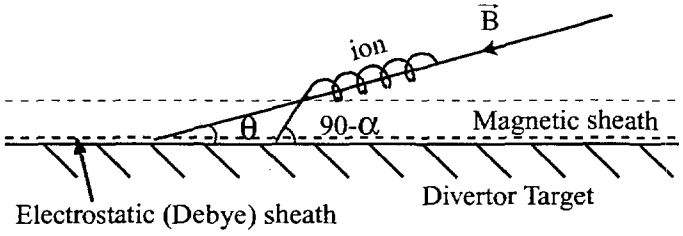

Figure 4

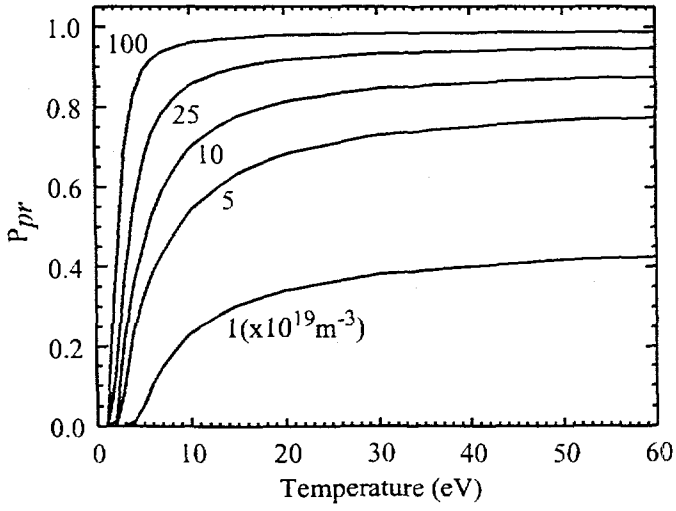

Figure 5

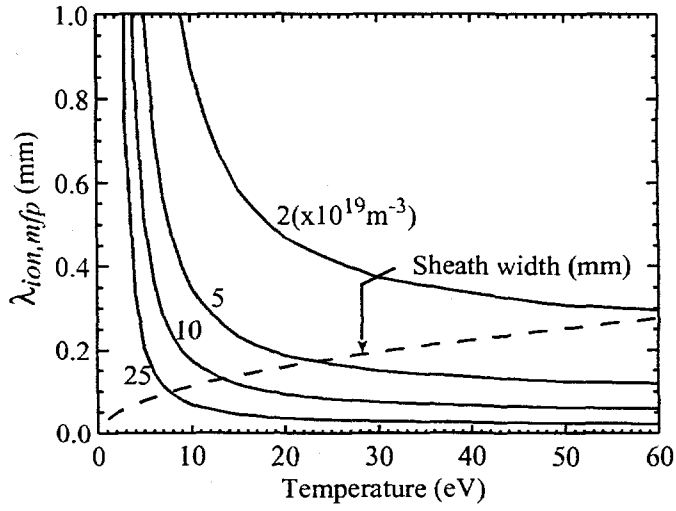

Figure 6

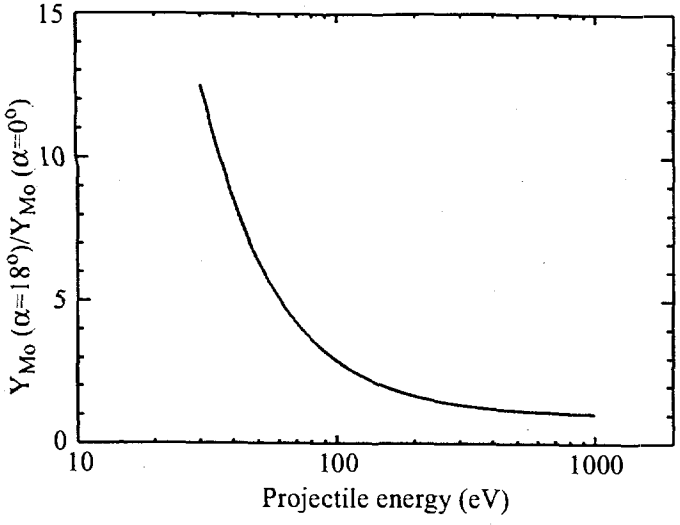

Figure 7

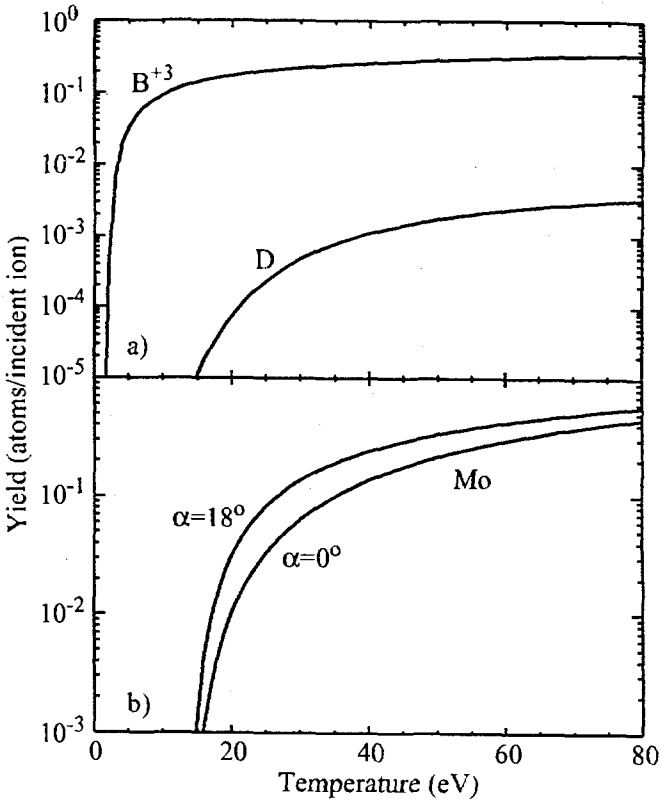

Figure 8

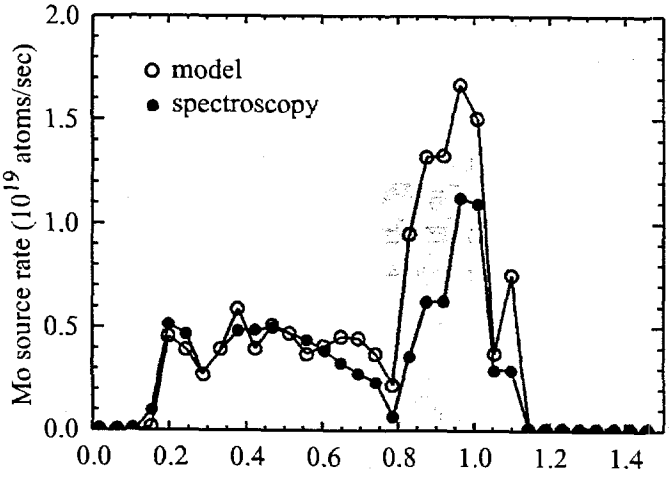

Figure 9

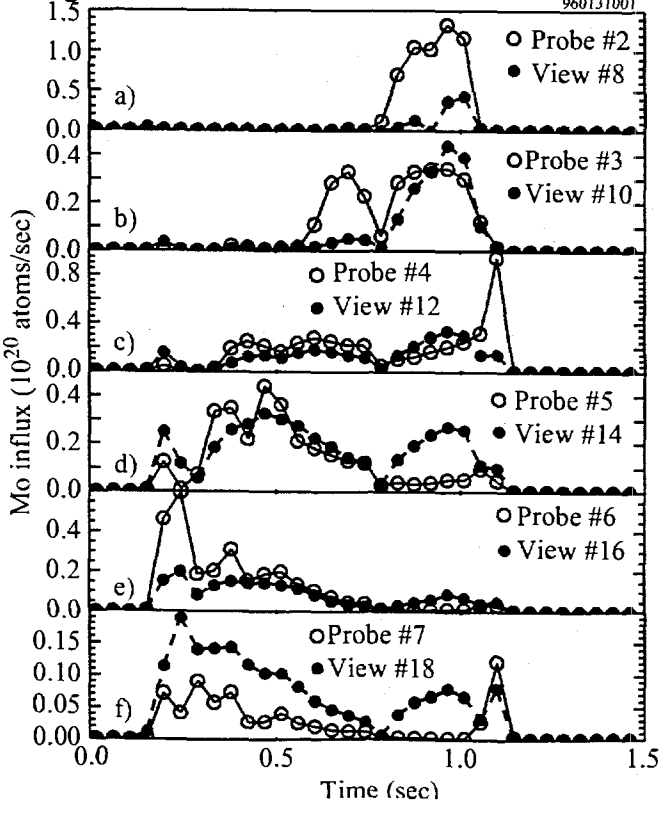

Figure 10

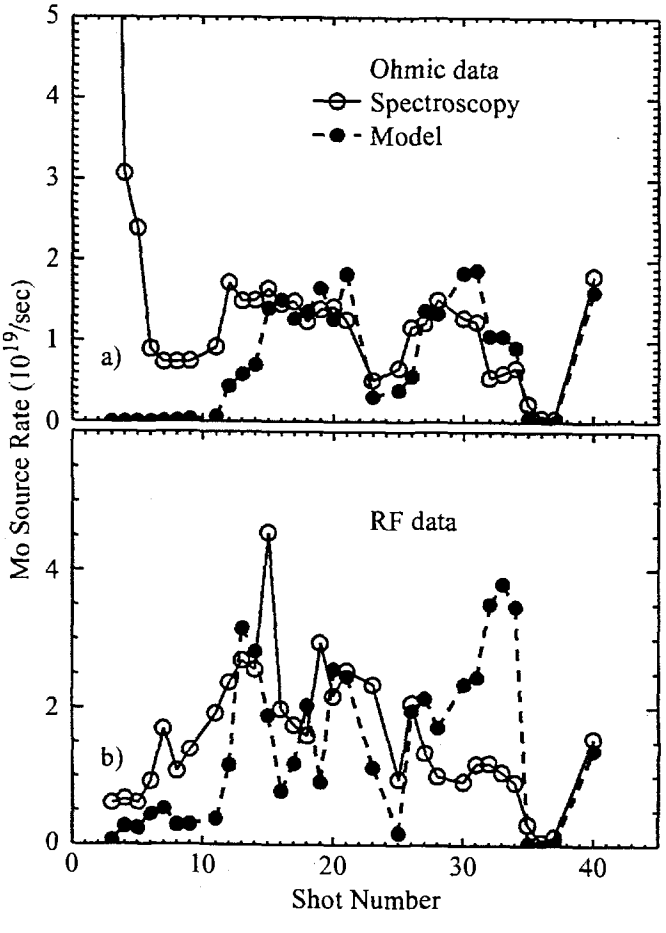

Figure 11

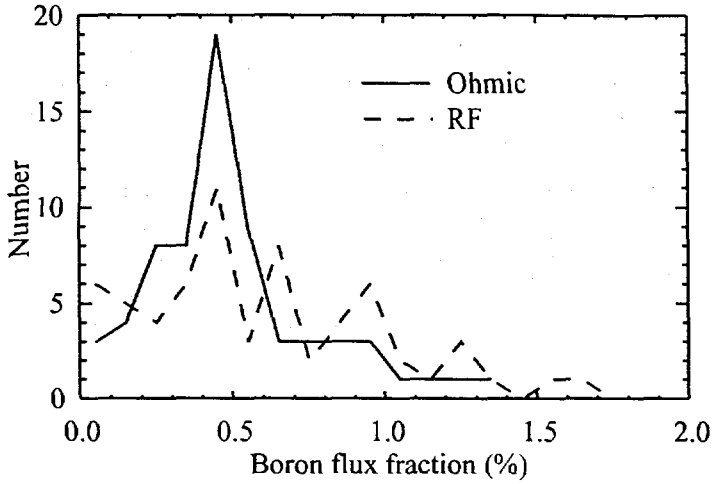

Figure 12

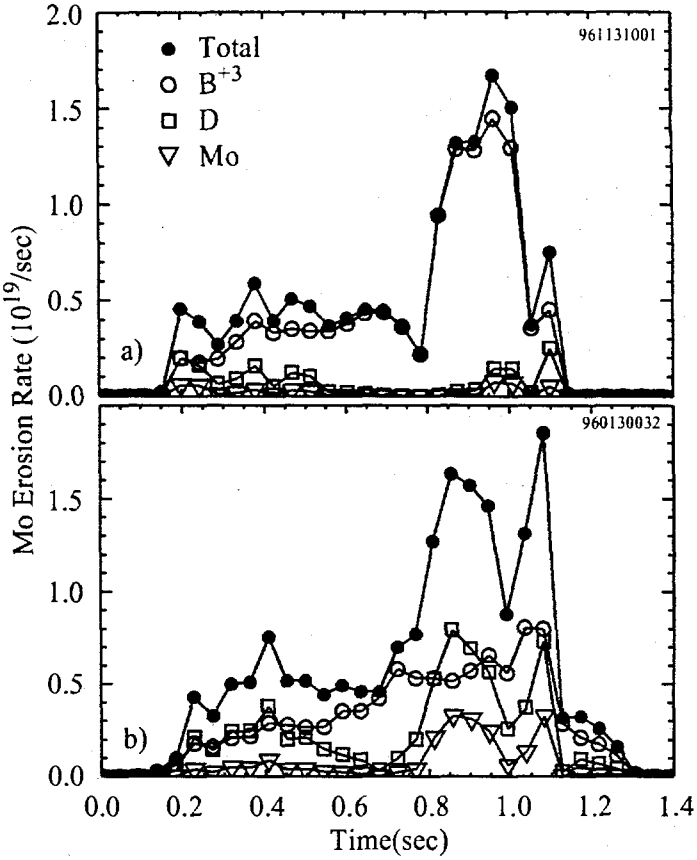

Figure 13

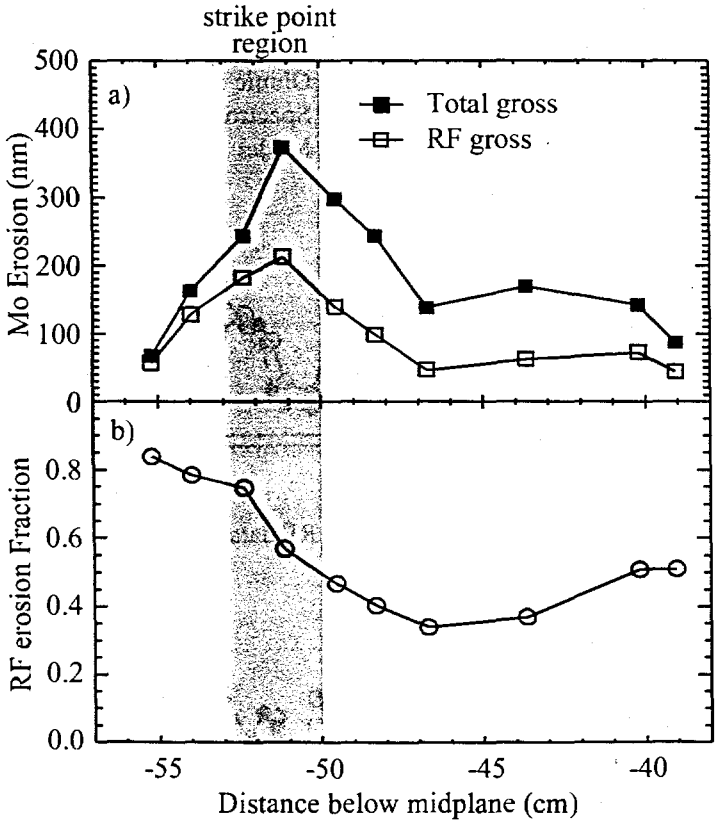

Figure 14